

Co-doped ZnO: synthesis and structural, electrical and optical properties

Hakan Çolak¹ · Orhan Türkoğlu²

Received: 22 June 2015 / Accepted: 25 August 2015 / Published online: 30 August 2015
© Springer Science+Business Media New York 2015

Abstract This paper reports the synthesis, crystal structure and electrical conductivity properties of Co-doped ZnO powders (in the range of 0.25–15 mol%). *I-phase* samples, which were indexed as single phase with a hexagonal (wurtzite) structure in the Co-doped ZnO system, were determined by X-ray diffraction. The solubility limit of Co ions in the ZnO structure was found to be 15 mol% at after heating at 950 °C. The impurity phase was determined to be Co₃O₄ at lower temperatures than 950 °C. The research focused on single *I-phase* samples which were synthesized at 950 °C. For *I-phase* samples (after heating at 950 °C), the lattice parameters *a* and *c* decreased with increasing Co concentration. Electrical conductivity of undoped ZnO and 15 mol% Co-doped ZnO (after heating at 950 °C) were found to be $7.8 \cdot 10^{-7}$ and $1.05 \cdot 10^{-4} \Omega^{-1} \text{cm}^{-1}$, respectively, at 25 °C and 1.15 and $37.15 \Omega^{-1} \text{cm}^{-1}$, respectively, at 950 °C. Thus, it appears that electrical conductivity slightly increases with Co doping. Also, activation energy of the all *I-phase* samples (after heating at 950 °C) was calculated and the values were found to be range from 0.774 to 1.201 eV. UV/vis absorption spectras of undoped and the all *I-phase* samples (after heating at 950 °C) were recorded and optical band gap values were found to be between 3.351 and 3.416 eV.

1 Introduction

Zinc oxide (ZnO) is one of the most important semiconductor materials due to its specific electrical, optical and mechanical properties [1]. ZnO normally occurs in the hexagonal crystal structure wherein both the Zn²⁺ and the O²⁻ ions are tetrahedrally coordinated. ZnO is a *n*-type semiconductor. This characteristic has been attributed to native defects such as oxygen vacancies and zinc interstitials [2]. ZnO is a commonly used material in photovoltaic devices as a transparent conductive oxide (TCO). For applications and control over the electrical and optical properties of ZnO, doping with different metals is needed [3]. In this way, the doping can enhance the properties of ZnO and enable the design of new applications [4]. The efficiency of the dopant element depends on its electronegativity and difference between ionic radius of its and zinc [5–7]. Besides, heating treatment is a widely used method to enhance any crystal quality and to study structural defects in materials. For semiconductors, heating treatment is also used to activate the doping materials [8]. During an heating process, dislocations and other structural defects will move in the material and adsorption/decomposition will occur on the surface, thus the structure and the stoichiometric ratio of the material will change, which effects the electrical and optical characteristics of ZnO [8, 9]. Also, it is well known that electrical conductivity of ZnO samples is controlled by intrinsic defects generated at high temperature and by the presence of dopants [5, 8].

There are many studies on transition metals doped ZnO samples and about their about magnetic properties [10–16]. Most of them which is on Co-doped ZnO concern magnetic properties [17–20].

In this work, Co-doped ZnO samples were synthesized by the solid state method at high temperatures. The all *I*-

✉ Hakan Çolak
hakancolak@karatekin.edu.tr; hakancolak38@gmail.com

¹ Department of Chemistry, Faculty of Science, Çankırı Karatekin University, 18100 Çankırı, Turkey

² Department of Chemistry, Faculty of Science, Erciyes University, 38039 Kayseri, Turkey

phase samples were characterized structural, morphological, electrical and optical properties. Solid state reaction was chosen because of its reproducibility, easy control and the ability to yield sufficient products for characterisation measurements [8, 12].

2 Experimental

Initially, solid mixtures of Co-ZnO in the range of $0.25 \leq x \leq 15$ mol% were prepared by mixing and homogenizing them using stoichiometric amounts of pure ZnO and metallic cobalt in an agate mortar. As starting materials, pure ZnO powders (99.9 % Fluka) and metallic Co powders (99.5 % Alfa Aesar) were used. Pure ZnO powders and powder mixtures were first calcined at 600 and 650 °C, respectively for 24 h. After grinding and homogenization, pre-annealed mixtures were heat treated in air at 700, 750, 800, 850, 900 and 950 °C 48 h in alumina crucibles, respectively. Finally, the samples were ground in an agate mortar to attain a uniform powder size. The samples were then analyzed using XRD on a Bruker AXS D8 advanced diffractometer. Diffrac Plus and Win-Index programs were used to obtain information about the crystal structures of samples. For a comparison with standard data, a PDF program (Maint Powder Diffraction Database Manager Software) was used. In all cases, XRD pattern of the single phased samples could be indexed on basis of a hexagonal structure in the Co-ZnO system. Single phase was named as *I-phase*. The other samples, which were outside the solubility range, were heterogeneous solid mixtures having another phase that could be indexed other than hexagonal. Morphologies of both non-annealed and annealed ZnO (at 950 °C) and doped ZnO samples (annealed at 950 °C) were observed using a scanning electron microscope (SEM, LEO 440). After pressing them into pellets of 0.1 cm thickness (*t*) and 1.3 cm in diameter (*d*) under 6 MPa pressure the samples were calcined at 950 °C for 24 h in air. After this heat treatment, XRD measurements showed no phase change in hexagonal samples. Average grain sizes were calculated using Image-Pro Plus 5.0 program by analysing the SEM micrographs. For this purpose, 10 grains were selected at random from each SEM image [8]. Electrical conductivity (σ) measurements of *I-phase* samples (after heating at 950 °C) were made using four probe method. As in SEM measurements, these samples were also pressed into circular disks. To reduce contact resistance, fine platinum wires were directly attached to the sample surface. The measurements performed in air at between 25 and 950 °C. All experimental data were obtained by a Keithley 2400 sourcemeter and a Keithley 2700 electrometer which were controlled by a computer [8, 21]. UV/vis absorption

spectras of the *I-phase* samples were recorded in a wavelength range of 300–1000 nm at room temperature by Rayleigh UV-2601 model spectrophotometer. The samples were prepared for measurements by dissolving 0.01 g powders in 50 mL doubly distilled water and keeping the suspensions in an ultrasonic bath for 10 min [22, 23] and the all suspensions were transparent.

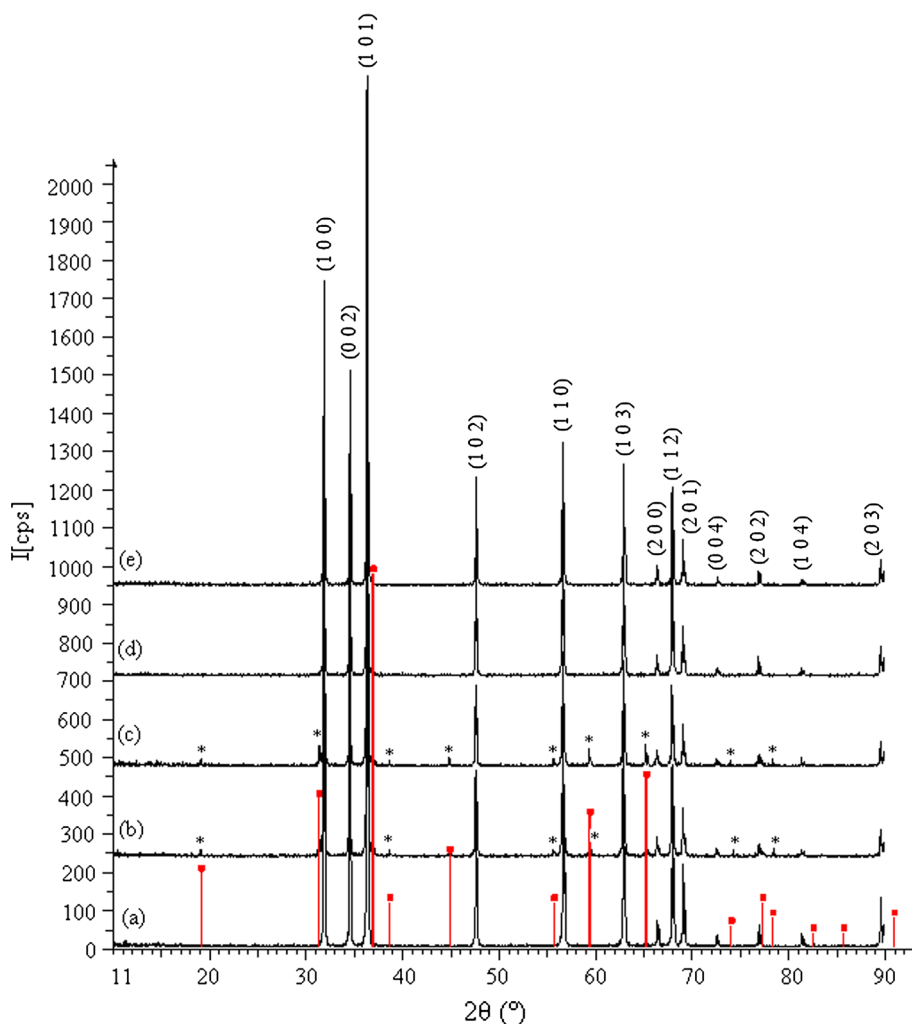
3 Results and discussion

3.1 XRD studies

To investigate the solubility of Co ions in ZnO structure, different compositions of Co-doped ZnO system were annealed at varying temperatures. Figure 1 shows the XRD patterns of undoped ZnO (after heating at 950 °C), 10 mol% Co-doped ZnO samples (after heating at 750 and 950 °C) and 15 mol% Co-doped ZnO samples (after heating at 850 and 950 °C). Figure 1a, d, e display similar patterns, which can be indexed to the hexagonal ZnO structure. The peak start to appear at $2\theta = 34.44^\circ$, which correspond to the (002) directions of the hexagonal structure [24]. For 10 mol% (after heating at 750 °C) and 15 mol% (after heating at 850 °C) Co-doped ZnO samples, the XRD patterns show extra peaks which indicate Co_3O_4 , (PDF no: 09-0418) [18, 19, 25]. The XRD patterns of other *I-phase* samples, which were synthesized at other temperatures, have quite similar patterns to given in Fig. 1. At lower temperatures than 950 °C, for some stoichiometric amounts, the XRD measurements revealed that coexistence of the *I* and *II* phase (*I* + *II*, heterogeneous solid mixtures). It is to be noted that no indication of Co metal impurities is observed in our samples. In the Co-doped ZnO system, observation of *I-phase* and heterogeneous solid mixtures depended on the reaction temperature and Co doping concentration, as presented in Table 1. The widest solubility limit of Co ions in ZnO structure was found to be 15 mol% after heating at 950 °C. The mobility of Co ions, which diffuse in ZnO tetrahedral sites, increase with heating temperature. Further, as the heating temperature increase the solubility limit is expected to increase because of an endothermic reaction [8, 9, 12]. In addition, both ionic radii and valence state are important factors in determining the solubility of the dopants [26]. In the rest of this study, we focused on *I-phase* samples which were synthesized after heating at 950 °C. The other *I-phase* samples which were synthesized at lower temperatures than 950 °C, and the multiphase samples (*I* + *II*) were excluded from this study.

The lattice constants of *I-phase* samples mostly ranged from 3.2489 to 3.2523 Å for the *a* parameter and from 5.2048 to 5.2080 Å for the *c* parameter. The deviation from

Fig. 1 XRD patterns for (a) undoped ZnO (after heating at 950 °C) and (b) 10 mol% (after heating at 750 °C), (c) 15 mol% (after heating at 850 °C), (d) 10 mol% (after heating at 950 °C) and (e) 15 mol% (after heating at 950 °C), (asterisk peaks of II phase, Co₃O₄)



the ideal hexagonal crystal is probably due to the lattice stability and ionicity [8, 27]. Figure 2a–b shows the dependence of the lattice parameters *a* and *c*, respectively, on the mol fraction of Co concentration. The lattice parameters of *I-phase* samples are smaller than undoped ZnO. Co²⁺ ions are substituted with Zn²⁺ ions which are in tetrahedral sites of the ZnO structure. The ionic radii of the Co²⁺ ion is 0.72 Å (when four-coordinated), while that of the Zn²⁺ ion is 0.74 Å [28]. Therefore, the decrease in lattice parameters *a* and *c* with Co doping can be explained by this ionic radii difference [8, 27].

3.2 Surface morphological studies

Figure 3 shows typical SEM micrographs of non-annealed and annealed (at 950 °C) undoped ZnO and some of the *I-phase* samples (after heating at 950 °C). The other *I-phase* samples (after heating at 950 °C) have quite similar images to given in Fig. 3. In the SEM micrographs, it can be seen a homogeneous grain distribution. From the micrographs, the

average grain sizes were calculated. For the non-annealed and annealed ZnO, they were found to be 0.63 and 1.03 μm, respectively. Average grain size of the annealed ZnO sample is obviously larger than that of non-annealed ZnO sample due to strain relaxation. The annealing process clearly produces a recovery of the crystal structure and increase of the grain size [29, 30]. As can be seen in the Fig. 3c–h, grains of the *I-phase* samples display homogeneous distribution. The average grain sizes of the *I-phase* samples are about 1 and 1.5 μm and they are not affected by Co doping concentration. Also, as can be seen in Fig. 3, grain boundaries are not formed and the grains are randomly agglomerate.

3.3 Electrical conductivity measurements

Total electrical conductivity is calculated using the following equation:

$$\sigma_T = \frac{I}{V} G^{-1} \tag{1}$$

Table 1 Observed phases in the binary system of Co-doped ZnO (in the range of 0.25–15 mol%)

Temp.(°C)	Co addition (mol%)																		
	0.25	0.50	0.75	1	2	3	4	5	6	7	8	9	10	11	12	13	14	15	
700	I	I	I	I + II	I + II	I + II	I + II	I + II	I + II	I + II	I + II	I + II	I + II	I + II	I + II	I + II	I + II	I + II	I + II
750	I	I	I	I	I	I + II	I + II	I + II	I + II	I + II	I + II	I + II	I + II	I + II	I + II	I + II	I + II	I + II	I + II
800	I	I	I	I	I	I	I + II	I + II	I + II	I + II	I + II	I + II	I + II	I + II	I + II	I + II	I + II	I + II	I + II
850	I	I	I	I	I	I	I + II	I + II	I + II	I + II	I + II	I + II	I + II	I + II	I + II	I + II	I + II	I + II	I + II
900	I	I	I	I	I	I	I	I	I	I	I	I	I + II	I + II	I + II	I + II	I + II	I + II	I + II
950	I	I	I	I	I	I	I	I	I	I	I	I	I	I	I	I	I	I	I

I Co-doped ZnO (hexagonal structure), *II* Co₃O₄

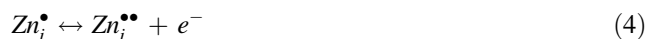
I + *II* heterogeneous solid mixtures

where *G* is the geometric resistivity correction factor [21]. There is a functional relation between sample geometry and voltage (*V*) and current (*I*) that influences the electrical conductivity [8, 21, 31, 32].

Electrical conductivity is related to the sample structure; any thermal treatment can modify structural and hence the electrical properties. On this basis, the study of temperature dependence of electrical properties may offer useful information about possible changes to the structure and characteristics of the Co-doped ZnO system [8, 33, 34].

Pelleted *I-phase* samples after heating at 950 °C were studied in the temperature range of 25–950 °C. Logσ–10³/*T* graphs were drawn in order to assess the dependence of conductivity on temperature. The graphs were compared with each other and, the electrical conductivity characteristics of *I-phase* samples were evaluated. The electrical conductivity plots of undoped ZnO and 0.50, 1, 3, 5, 7, 10, 13 and 15 mol% Co-doped ZnO samples (after heating at 950 °C) versus temperature are given in Fig. 4. The graphs of other *I-phase* samples (after heating at 950 °C) were quite similar to the curves given in this figure. As can be seen, the electrical conductivity of the all *I-phase* samples increases with measurement temperature, indicating semiconducting behaviour. As mentioned above, it is well known that electrical conductivity of undoped ZnO is controlled via intrinsic defects (namely, oxygen vacancy and interstitial zinc atoms) generated at high temperatures [5, 8].

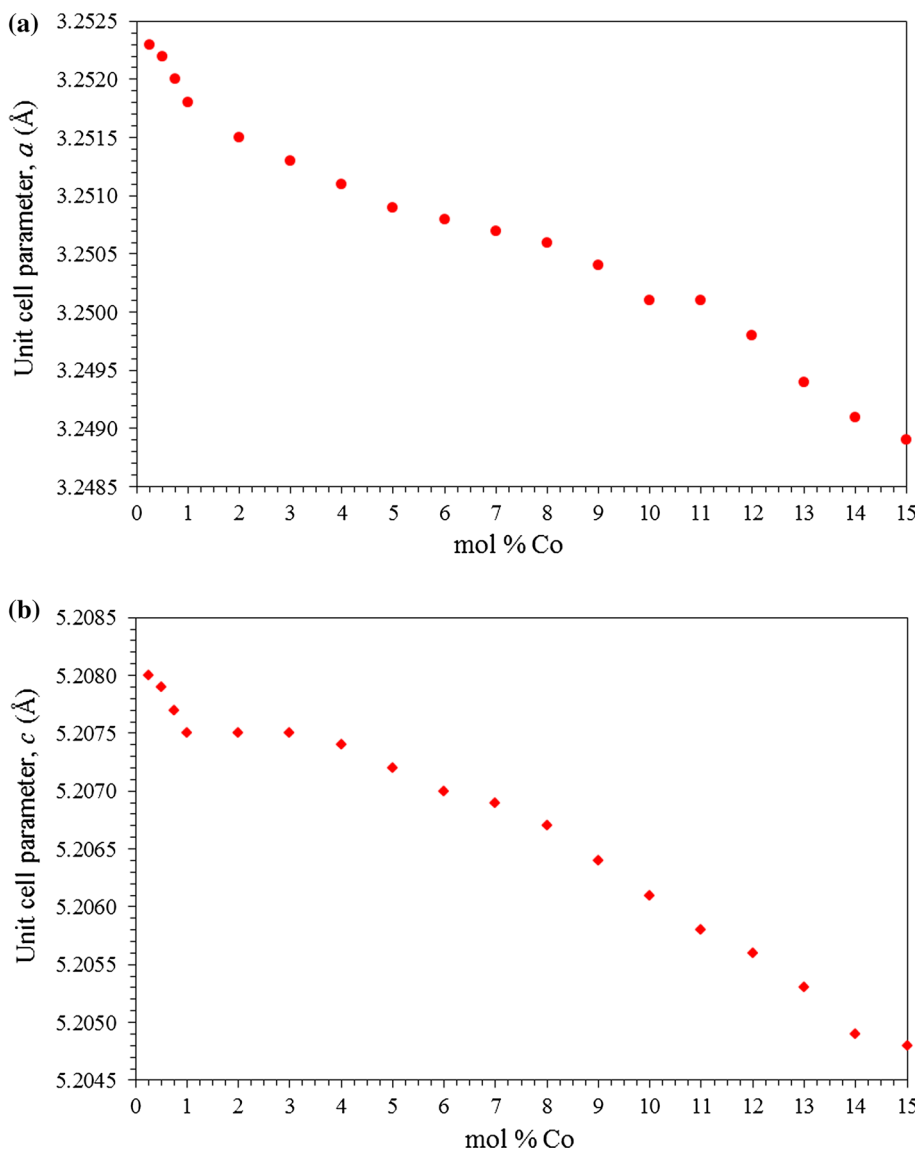
The increase in electrical conductivity with temperature can also be explained through the following reactions:



After the ionization reactions, the carrier concentration is increased by two extra electrons [35]. The electrical conductivity of the doped ZnO samples usually follows a mechanism in which the electrical charge (free electron or hole) jumps from one localized site to the next. Whenever a charge is moved to another site, the surrounding molecules respond to this perturbation with structural changes and the electron or hole is temporarily trapped. The charge stays at this site until it is thermally activated to migrate to another one. Also, there is another aspect for this charge hopping mechanism where the charge tends to associate with local defects [8, 36].

For undoped ZnO, 1 and 15 mol% Co-doped ZnO samples, the electrical conductivity values are 7.08×10^{-7} , 7.08×10^{-6} and $1.05 \times 10^{-4} \Omega^{-1} \text{cm}^{-1}$ at 25 °C, and 1.15, 1.51 and $37.15 \Omega^{-1} \text{cm}^{-1}$ at 950 °C, respectively. Figure 5 shows the electrical conductivity variation with Co doping concentration. As seen in this

Fig. 2 Change in the unit cell parameters of *I-phase* samples (after heating at 950 °C)



figure, the conductivity of the all *I-phase* samples slightly increases with increase of Co doping concentration.

3.4 Activation energy

In general for a semiconducting material, the electrical conductivity increases exponentially with temperature indicating conductivity is a thermally activated process. For doped semiconductors with low concentration of donors, hopping transport of carriers is expected between the nearest donors at low temperatures [8]. Total electrical conductivity can be expressed as:

$$\sigma = \sigma_0 \exp(-E_a/kT) \tag{5}$$

where σ is electrical conductivity at temperature, E_a is the activation energy, which corresponds to the energy difference between the donor level and the conduction level,

σ_0 is called the pre-exponential factor, k is the Boltzmann constant, and T is the absolute temperature [5, 6, 36, 37].

The activation energy can be calculated from the conductivity equation shown below

$$\ln(\sigma) = -\frac{E_a}{k} \frac{1}{T} + \ln(\sigma_0) \tag{6}$$

The slope of the linear part of the Arrhenius curve of the $\log\sigma-1/T$ graph is equal to $-E_a/k$. For the studied temperature range, the all samples have Arrhenius-type electrical conductivity. The activation energy values of the all *I-phase* samples are range between 0.774 and 1.201 eV. The activation energy (E_a) plotted as function of Co doping concentration (in Fig. 6) reveals that E_a decreases with Co doping concentration. This can be explained as follows: the activation energy for thermally activated band conduction depends on donor concentration and impurity levels. An

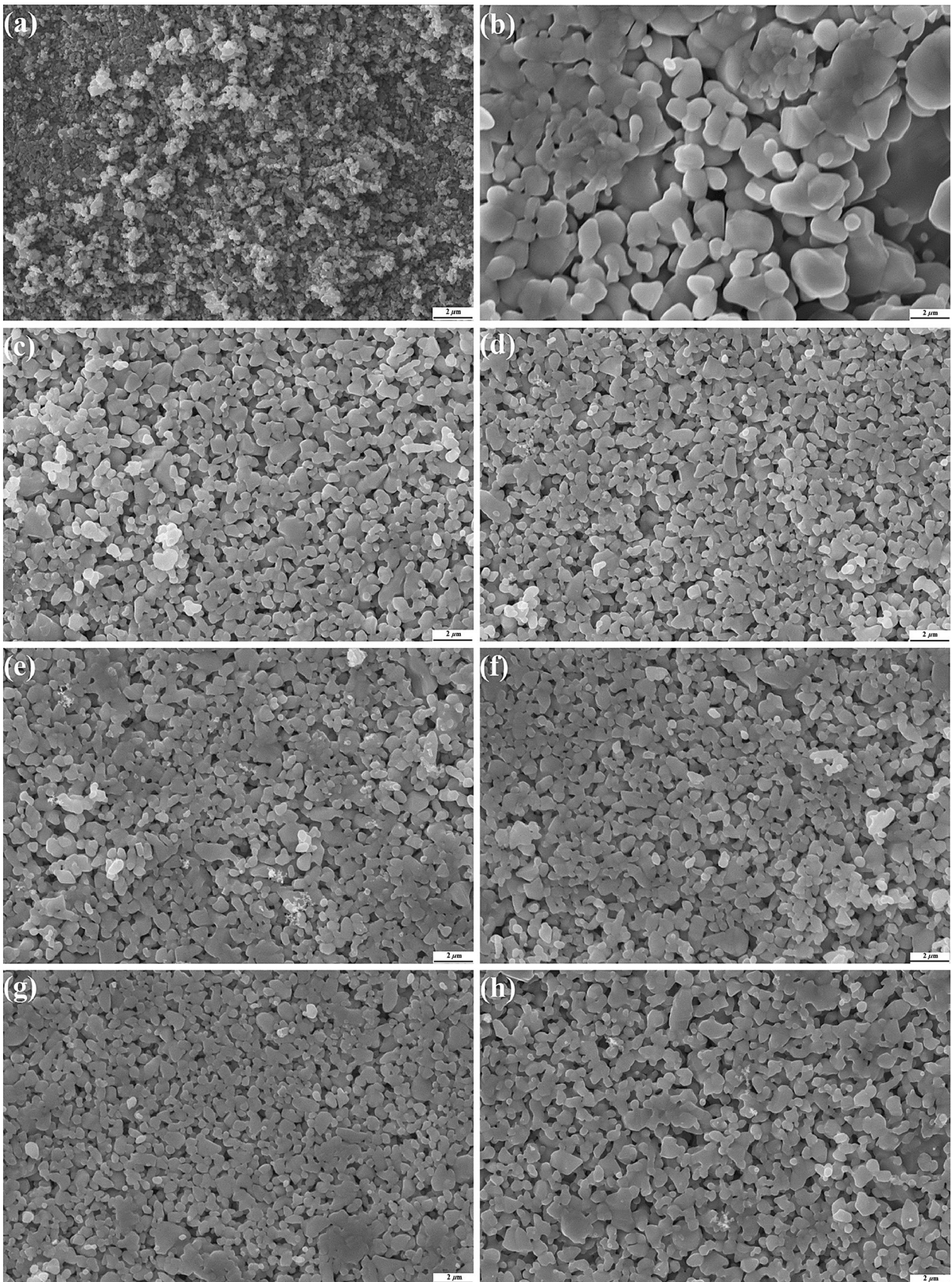


Fig. 3 SEM micrographs of some *I-phase* samples: **a** undoped ZnO (non-annealed) and **b** undoped ZnO (annealed at 950 °C), **c** 0.25, **d** 0.50, **e** 7, **f** 8, **g** 14 and **h** 15 mol% Co-doped ZnO (after heating at 950 °C)

increase in donor carrier concentration brings the Fermi level up in the energy gap and results in a decrease of the activation energy [8, 38].

3.5 Optical study

The optical transmittance spectrums of undoped and 0.25, 0.50, 1, 3, 5, 7, 9, 10, 13 and 15 mol% Co doped ZnO are shown in Fig. 7. The spectras of the other *I-phase* samples

(after heating at 950 °C) were similar to the spectras given in this figure. From Fig. 7, it is shown that a region of strong transparency is located between 400 and 1000 nm. The all *I-phase* samples exhibit an average optical transparency over 70–89 % in the visible range. Figure 8 shows the plots of $(\alpha E)^2$ versus photon energy (E , eV) for *I-phase* samples. Optical band gaps (E_g) were determined from this plots. The band gaps were found to be vary from 3.351 to 3.416 eV as shown in Table 2. It was observed a decrease with increasing cobalt doping concentration [39]. This may be attributed to the sp–d exchange interactions between the band electrons and the localized d electrons of the Co^{2+} ions substituting Zn^{2+} ions [40, 41]. This is a clear evidence that cobalt ions enter in the tetrahedral sites of the

Fig. 4 Electrical conductivity plots for undoped ZnO and some *I-phase* samples (after heating at 950 °C)

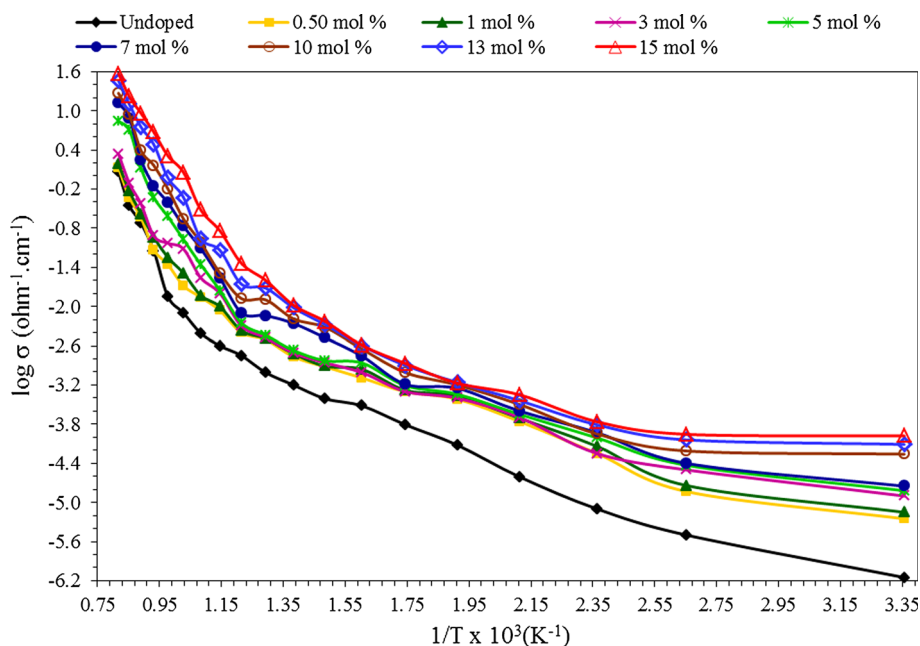


Fig. 5 Electrical conductivity variation of *I-phase* samples versus Co doping concentration (after heating at 950 °C)

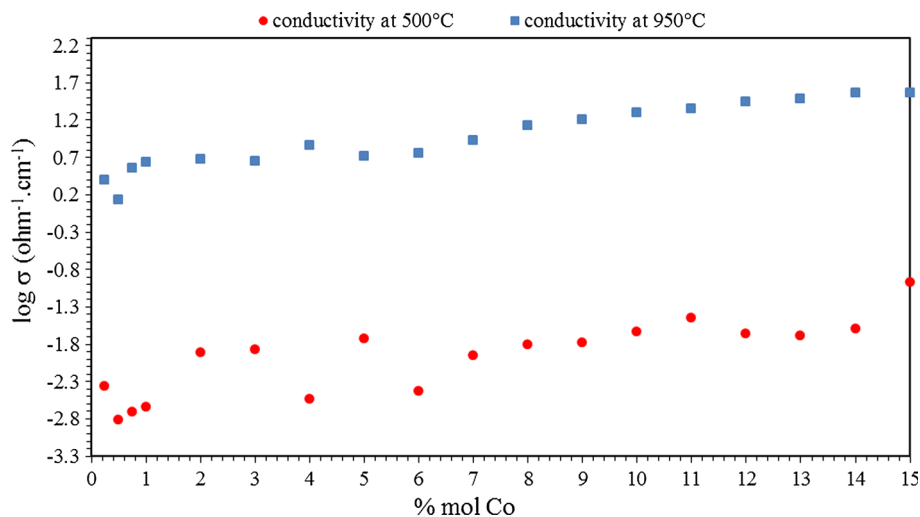


Fig. 6 Doping concentration effect on activation energy of *I-phase* samples (after heating at 950 °C)

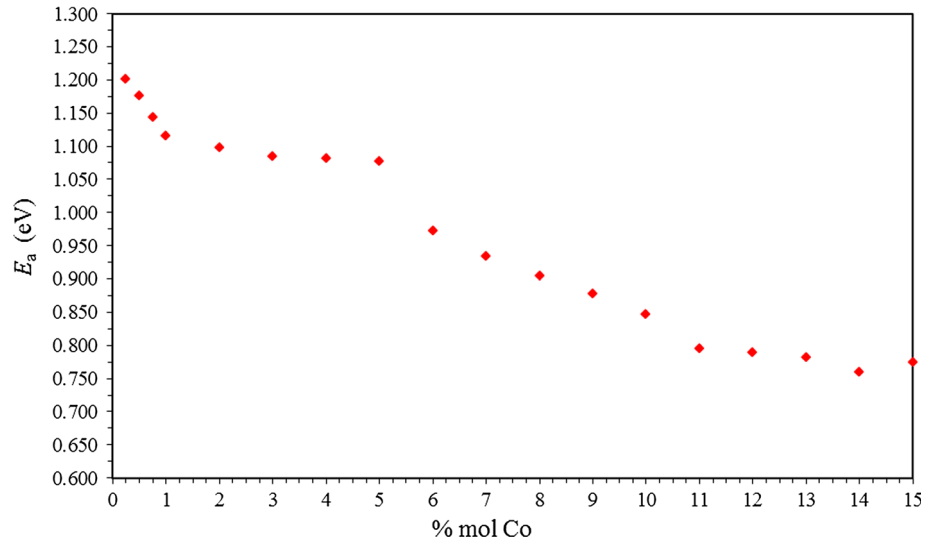


Fig. 7 Optical transmittance spectrum of undoped ZnO (after heating at 950 °C) and some *I-phase* samples (after heating at 950 °C)

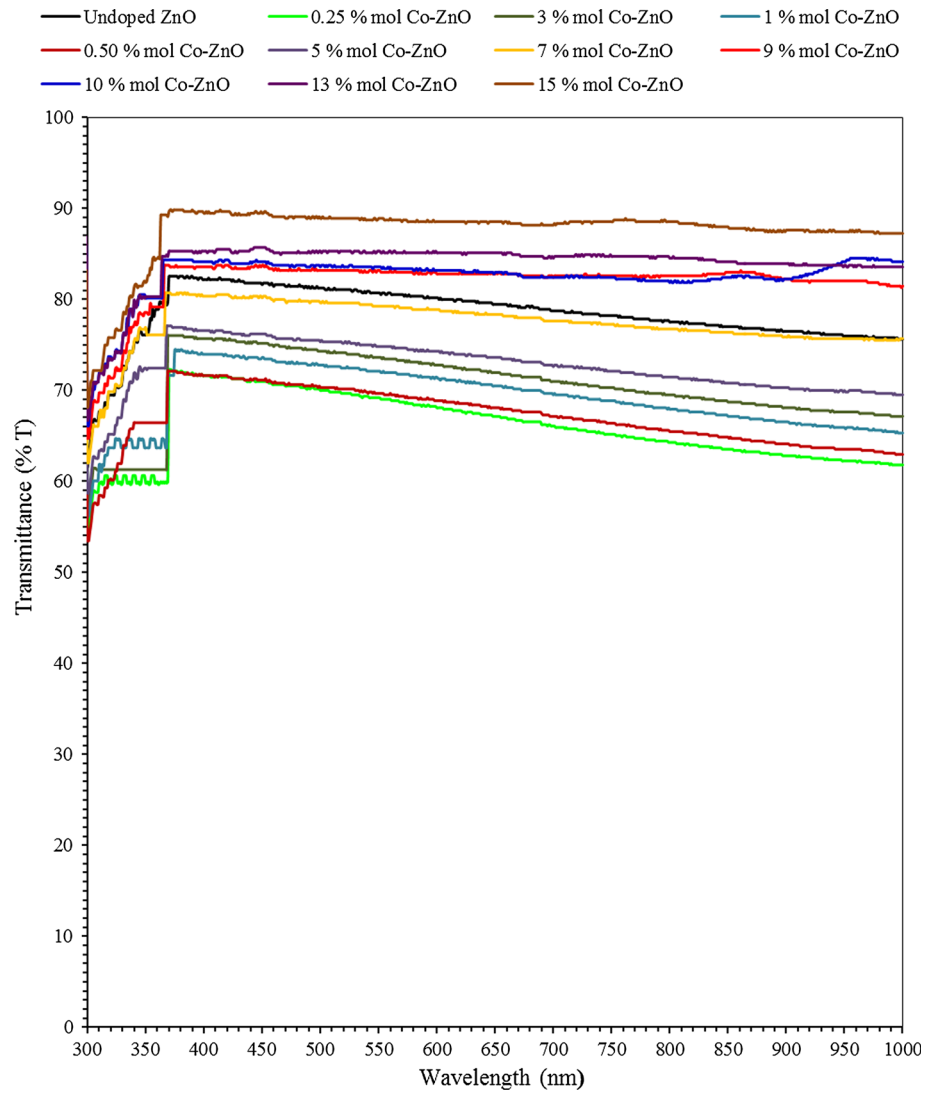


Fig. 8 The plot of the graph of $(\alpha E)^2$ versus photon energy (eV) for: **a** undoped ZnO, 3, 5 and 7 mol%, **b** 10, 13 and 15 mol% Co-doped ZnO (after heating at 950 °C)

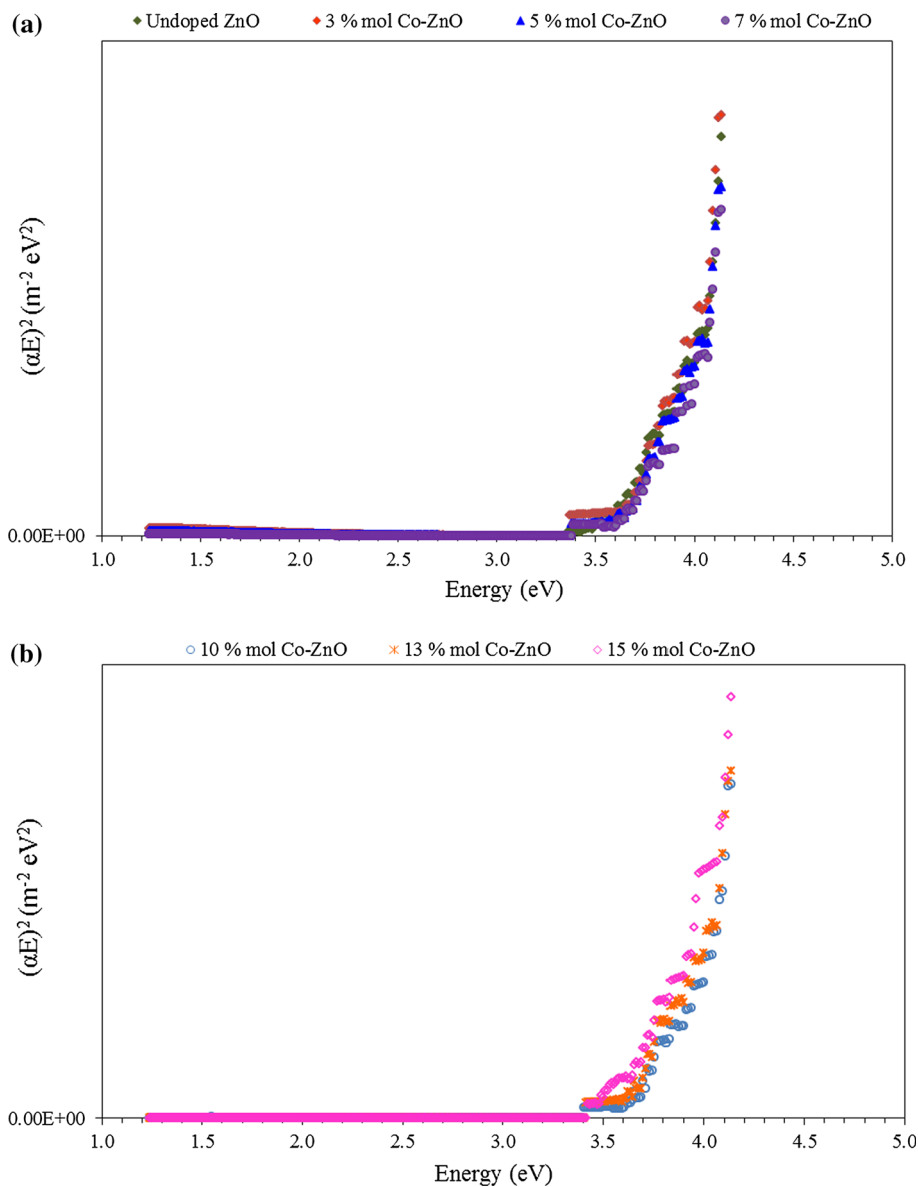


Table 2 The band gap values of *I-phase* samples (after heating at 950 °C)

	Doping concentration of Co (mol%)								
	0.25	0.50	0.75	1	2	3	4	5	6
Band gap (eV)	3.416	3.406	3.397	3.396	3.395	3.387	3.385	3.384	3.378
	Doping concentration of Co (mol%)								
	7	8	9	10	11	12	13	14	15
Band gap (eV)	3.378	3.375	3.372	3.369	3.365	3.364	3.360	3.357	3.351

wurtzite structure as Co^{2+} rather than forming metallic form which is consistent with the XRD data (Fig. 1). The values of electrical conductivity (σ) are found to increase with the increase in cobalt doping percentage. This behaviour of the conductivity could be understood from the fact that with the increase in Co doping. Initially the Co^{2+} ions

occupy interstitial position thus increasing the scattering from the defects. While at higher doping, the carrier concentration become much larger and it dominates the contribution from scattering and gives rise to increase in conductivity [42]. So, observed all results are in good agreement for our samples.

4 Conclusion

Co-doped ZnO powders were synthesized by using a solid state reaction method with metallic Co powder and commercial pure ZnO powder. The XRD analysis results indicated that all *I-phase* samples in the Co-doped ZnO system (in the range of 0.25–15 mol% after heating at 950 °C) had a hexagonal structure, namely the solubility limit of Co ions in ZnO lattice at this temperature is 15 mol%. The lattice constants of *I-phase* samples decreased with Co doping concentration. The decrease in the lattice parameters *a* and *c* can be explained by ionic radii difference. For undoped and Co-doped ZnO samples (after heating at 950 °C), electrical conductivity increased with heat treatment and cobalt doping concentration. From UV/vis spectras, the optical band gaps of the all *I-phase* samples were found and observed a decrease with increasing of Co doping concentration.

Acknowledgments This study was financially supported by the Research Foundation of Erciyes University (Kayseri, Turkey).

References

1. S. Ghosh, P. Srivastava, B. Pandey, M. Saurav, P. Bharadwaj, D.K. Avasthi, D. Kabiraj, S.M. Shivaprasad, *Appl. Phys. A* **90**, 765 (2008)
2. B.J. Copa B, Phd. Dissertation, North Carolina State University, USA, 2003
3. F. Fang, A.M.C. Ng, X.Y. Chen, A.B. Djuricic, Y.C. Zhong, K.S. Wong, P.W.K. Fong, H.F. Lui, C. Surya, W.K. Chan, *Mater. Chem. Phys.* **125**, 323 (2011)
4. R.A. Mereu, A. Mesaros, M. Vasilescu, M. Popa, M.S. Gabor, L. Ciontea, T. Petrisor, *Ceram. Int.* **39**, 5535 (2013)
5. A. Sawalha, M. Abu-Abdeen, A. Sedky, *Phys. B Condens. Matter.* **404**, 1316 (2009)
6. P. Nunes, E. Fortunato, P. Vilarinho, R. Martins, *Vacuum* **64**, 281 (2002)
7. R. Wang, A.S. Sleight, *Chem. Mater.* **8**, 433 (1996)
8. H. Colak, O. Turkoglu, *Mater. Sci. Semicond. Proc.* **16**, 712 (2013)
9. L. Wang, Y. Pu, W. Fang, J. Dai, C. Zheng, C. Mo, C. Xiong, *Thin Solid Films* **491**, 323 (2005)
10. G.Y. Ahn, S.I. Park, S.J. Kim, C.S. Kim, *J. Magn. Magn. Mater.* **304**, 498 (2006)
11. A.Y. Polyakov, A.V. Govorkov, N.B. Smirnov, N.V. Pashkova, S.J. Pearton, K. Ip, R.M. Frazier, C.R. Abernathy, D.P. Norton, J.M. Zavada, R.G. Wilson, *Mater. Sci. Semicond. Process* **7**, 77 (2004)
12. X. Mao, W. Zhong, Y. Du, *J. Magn. Magn. Mater.* **320**, 1102 (2008)
13. G. Pei, C. Xia, S. Cao, J. Zhang, F. Wu, J. Xu, *J. Magn. Magn. Mater.* **302**, 340 (2006)
14. X. Feng, *J. Phys. Condens. Matter* **16**, 4251 (2004)
15. S.J. Pearton, D.P. Norton, M.P. Mill, A.F. Hebard, J.M. Zavada, W.M. Chen, I.A. Buyanova, *IEEE Trans. Electron Devices* **54**, 1040 (2007)
16. S. Thota, T. Dutta, J. Kumar, *J. Phys. Condens. Matter* **18**, 2473 (2006)
17. L.C. Damonte, M.A. Hernandez-Fenollosa, M. Meyer, L. Mendoza-Zelis, B. Mari, *Phys. B* **398**, 380 (2007)
18. Y. Wang, L. Sun, L.G. Kong, J.F. Kang, X. Zhang, R.H. Han, *J. Alloy. Compd.* **423**, 256 (2006)
19. M. Wei, D. Zhi, L. Judith, D. Macmanus, *Scripta Mater.* **54**, 817 (2006)
20. C.B. Fitzgerald, M. Venkatesan, J.G. Lunney, L.S. Dorneles, J.M.D. Coey, *Appl. Surf. Sci.* **247**, 493 (2005)
21. S. Yilmaz, O. Turkoglu, I. Belenli, *Mater. Chem. Phys.* **112**, 472 (2008)
22. S. Husain, L.A. Alkhtaby, E. Giorgetti, A. Zoppi, M.M. Miranda, *J. Lumin.* **145**, 132 (2014)
23. H. Colak, *J. Mater. Sci. Mater. Electron* **26**, 784 (2015)
24. A.J. Chen, X.M. Wu, Z.D. Sha, L.J. Zhuge, Y.D. Meng, *J. Phys. D Appl. Phys.* **39**, 4762 (2006)
25. N.T.T. Hien, N.X. Dai, N.A. Tuan, V.N. Thuc, V.T. Son, P.T. Mai, *Proceedings of the Eighth German-Vietnamse Seminar on Physics and Engineering*, Erlangen, 3–8 April 2005
26. H. Colak, O. Turkoglu, *J. Mater. Sci. Technol.* **27**, 944 (2011)
27. U. Ozgur, Y.I. Alivov, C. Liu, A. Teke, M.A. Reshchikov, S. Dogan, V. Avrutin, S.J. Cho, H. Morkoc, *J. Appl. Phys.* **98**, 041301 (2005)
28. R.C. Weast, *Handbook of chemistry and physics*, 56. ed., Crc Press, Florida, 1975–1976
29. S.Y. Chu, T.M. Yan, S.L. Chen, *Ceram. Int.* **26**, 733 (2000)
30. X.X. Wei, C. Song, K.W. Geng, F. Zeng, B. He, F. Pan, *J. Phys. Condens. Matter* **18**, 7471 (2006)
31. S. Yilmaz, O. Turkoglu, M. Ari, I. Belenli, *Ceramica* **57**, 185 (2011)
32. D.K. Schroder, *Semiconductor Material and Device Characterization*, 3:8 (John Wiley & Sons, USA, 2006)
33. M. Girtan, G.G. Rusu, S.D. Seignon, M. Rusu, *Appl. Surf. Sci.* **254**, 4179 (2008)
34. H. Colak, O. Turkoglu, *Synthesis. J. Mater. Sci. Technol.* **28**, 268 (2012)
35. J. Han, A.M.R. Senos, P.Q. Mantas, *J. Eur. Ceram. Soc.* **22**, 49 (2002)
36. M.S. Hossain, R. Islam, K.A. Khan, *Chalcogenide Lett.* **5**, 1 (2008)
37. Y. Natsume, H. Sakata, *Thin Solid Films* **372**, 30 (2000)
38. R. Kumar, N. Khare, *Thin Solid Films* **516**, 1302 (2008)
39. J. El Ghoul, M. Kraini, O.M. Lemine, L. El Mir, *J. Mater. Sci. Mater. Electron* **26**, 732 (2015)
40. J. Diouri, J.P. Lascaray, M.E. Amrani, *Phys. Rev. B Condens. Matter* **31**, 7995 (1985)
41. G. Vijayaprasath, R. Murugan, T. Mahalingam, G. Ravi, *J. Mater. Sci. Mater. Electron.* **26**, 3346 (2015)
42. G. Singh, S.B. Shrivastava, V. Ganesan, *J. Chem. Eng. Mat. Sci.* **4**, 1 (2013)